ELSEVIER

Journal of Chromatography A, 827 (1998) 281–293

JOURNAL OF CHROMATOGRAPHY A

Comparison of protein adsorption isotherms and uptake rates in preparative cation-exchange materials

Calendula Chang[1], Abraham M. Lenhoff*

Center for Molecular and Engineering Thermodynamics, Department of Chemical Engineering, University of Delaware, Newark, DE 19716, USA

Abstract

Adsorption isotherms and effective diffusivities of lysozyme in a set of six preparative cation-exchange stationary phases were determined from batch uptake data in a stirred vessel. Both a pore diffusion and a homogeneous diffusion model were used in estimating diffusivities, with the isotherms fitted to a non-Langmuirian analytical isotherm equation. The capacities inferred from the isotherms are found to be correlated with the surface area accessible to lysozyme, the effective surface concentrations obtained being in agreement with values measured by different methods in various non-chromatographic systems. The pore diffusivities show systematic trends with protein and salt concentration, and effects of pore size and connectivity are also evident. Some trends in the homogeneous diffusivities are quite different to those in the pore diffusivities, but these differences largely disappear when the homogeneous diffusivities are rescaled to account for adsorption equilibrium behavior. Additional information is required to elucidate further the mechanisms of coupled diffusion and adsorption in stationary phases. © 1998 Elsevier Science B.V. All rights reserved.

Keywords: Adsorption isotherms; Diffusion coefficients; Pore structure; Stationary phases, LC; Preparative chromatography; Proteins; Lysozyme

1. Introduction

A wide variety of suitable stationary phases for large-scale protein chromatography is available [1,2] with different base matrix properties and different functional group chemistry, even for the same chromatographic mode. Optimizing a given separation involves selecting a stationary phase and finding the most suitable operating conditions. Stationary phase selection is usually done by extensive empirical screening [3], and the subsequent adjustment of operating conditions is accomplished largely heuristically as well. In order to place these tasks on a more rational foundation, mechanistic relationships are required between separation performance and physicochemical parameters, including ones that characterize the structure and properties of the protein, the stationary phase and the eluent. We describe elsewhere [4,5] our progress in developing such relationships for protein retention, whilst the present paper addresses full isotherms and diffusional characteristics.

The measures of performance by which preparative and production-scale chromatography are judged differ from those that are relevant to analytical separations. For instance, such issues as capacity, recovery and throughput are critical to large-scale separations. Although some of these issues are related to corresponding ones of concern at the

*Corresponding author. Fax: +1-302-831-4466; e-mail: lenhoff@che.udel.edu

[1]Current address: Wafer-Tech, 5509 NW Parker St., Camas, WA 98607, USA.

0021-9673/98/$ – see front matter © 1998 Elsevier Science B.V. All rights reserved.
PII: S0021-9673(98)00796-1

analytical scale, the constraints at large scale typically require different approaches to optimization. An example pertinent to the transport issues of interest here is that of throughput. For analytical separations the requirement is for rapid analysis, and this is accomplished by using small and sometimes non-porous stationary phase particles. For large-scale separations, however, these strategies conflict with capacity demands: small particles lead to an unacceptably high pressure drop in larger columns, and non-porous or pellicular particles have intrinsically low capacities. Thus preparative separations are generally performed using large (tens to hundreds of μm in diameter) porous particles [1,2].

The most obvious approach to increasing throughput is to operate at a high flow rate, and the linear velocities used in practice may be on the order of hundreds of cm/h. Where the optimum lies for each separation depends on a trade-off of throughput against selectivity and recovery. However, the flow rates used correspond to plate heights well beyond the minimum in a Van Deemter plot, because of the large particle sizes and the resulting long intraparticle diffusion distances. There is thus an incentive to obtain a better quantitative understanding of intraparticle diffusion, both for straightforward comparative studies and for use in more detailed column models [6–8]. It is also desirable to elucidate the relationship of intraparticle diffusion to the stationary phase structure, in order to aid in selection of stationary phases and operating conditions, as well as ultimately in stationary phase design.

Intraparticle diffusion is inherently difficult to describe because of the complex mix of phenomena occurring within the pore structure. Even in the absence of adsorption, three distinct effects must be considered:

(1) *Hindrance:* A macromolecule diffusing within a pore is retarded by hydrodynamic interactions with the bounding pore wall. This situation has been analyzed in detail for idealized model situations, generally a sphere moving in a cylindrical pore [9].

(2) *Partitioning:* The average volumetric concentration of macromolecules within the pore space is lower than that in the surrounding bulk solution because the macromolecules are sterically excluded from the immediate vicinity of the pore walls. The partition coefficient can be estimated from simple geometric arguments for idealized pore shapes [10,11].

(3) *Tortuosity:* Diffusion between two points in a convoluted pore space is retarded by two related effects relative to that along a linear path. First, the diffusion path is longer, and second, the concentration gradient is less steep. The result is a so-called tortuosity factor that has been shown empirically to slow diffusion by a factor that is usually between 2 and 6 [12].

Realistically describing both restricted diffusion and non-linear adsorption simultaneously within the heterogeneous geometrical and functional milieu of the pore space is impossible at present except in a highly idealized fashion [13]. Thus the preferred approach is to measure isotherms and intraparticle diffusion rates, and it is such experiments that we report here for ion-exchange materials. Our work differs from previous results in two respects. First, whereas most previous studies were based on a single stationary phase, we have used a set of commercial ion-exchange materials of which we have previously characterized structural [4] and retention [5] characteristics. Thus we are able to perform a more extensive comparative study to help understand how intraparticle transport is related to structural parameters. Second, we have obtained uptake results over a range of protein and salt concentrations that help elucidate the coupling between retention and transport within the stationary phase.

Intraparticle diffusion measurements are most commonly performed via stirred-batch uptake experiments; this is also the approach used here. Since the rate of uptake into the chromatographic particles is followed by measuring the residual protein concentration in the supernatant, intraparticle diffusion coefficients must be estimated within the framework of a suitable transport model, of which various degrees of complexity are possible [7]. Several simpler limiting models were compared by Johnston and Hearn [14], but for a realistic description of the transport aspects only the most complex of the models they examined [15] is satisfactory. The transport formulation on which it is based has been used for many years, including in column models; it accounts for mass transfer to the surface of the particles, diffusion within the pore lumen, and

adsorption, characterized by an isotherm or sometimes by a kinetic description, on the pore walls. Such models have been used to estimate diffusivities in such media as ion-exchange [16–18], affinity [19] and hydrophobic interaction [20] phases.

Transport models of this kind often fit uptake data quite well, and where they do not, alternative formulations, e.g., ones that allow for simultaneous pore and surface diffusion [21,22] or for ''homogeneous'' diffusion of adsorbed protein [17,23], may be more successful. How accurately any transport model reflects the actual physical events within porous particles is, however, open to question. In this work we have made use of both the pore diffusion and the homogeneous diffusion models, and in both cases it is possible to obtain reasonable fits of the experimental data. Thus model discrimination is not feasible, and the principal value in our results lies mainly in the comparison that is provided of a wide range of different stationary phases. Previous reports have provided only limited comparisons of this kind. For instance, Johnston and Hearn [14] compared uptake of three proteins into three DEAE anion exchangers within the framework of a number of different models, but only for two initial protein concentrations and under very low salt concentrations. Weaver and Carta [17] found significant differences in lysozyme uptakes into two cation exchangers, but these experiments were intended to probe novel structural features that might be expected to lead to unusual uptake behavior in these materials.

2. Experimental

2.1. Materials

Hen egg white lysozyme (L-6876) was obtained from Sigma (St. Louis, MO, USA). All solutions were prepared in ultrapure deionized (18.2 MΩ cm) water from a Millipore Milli-Q system. Experiments were performed in 10 mM phosphate buffer at pH 7 containing sodium chloride at a concentration of 0, 0.1 or 0.2 M. All buffers were filtered through 0.2 μm membranes (Gelman Sciences Supor) and degassed with helium prior to use. Protein solutions were syringe-filtered through 0.45 μm membranes to remove large protein aggregates.

Six commercially available strong cation-exchange resins were used. Batch adsorption experiments were performed with Toyopearl SP650C and SP550C (TosoHaas, Montgomeryville, PA, USA), SP Sepharose FF (Pharmacia Biotech, Uppsala, Sweden), Fractogel EMD SO_3^- 650M (EM Separations, Hawthorne, NY, USA), Bakerbond Carboxy-Sulfone (Mallinckrodt Baker, Phillipsburg, NJ, USA), and SP Spherodex M (Biosepra Inc., Marlborough, MA, USA). These six cover a range of sorbent base matrices (vinyl polymers, agarose, silica), mean particle and pore sizes, and ion binding capacities; some of these properties are summarized in Table 1. The two TosoHaas materials are based on the same methacrylate chemistry, but the 650 material has a larger mean pore size than the 550. EMD SO_3^- has the same base matrix as TosoHaas 650, but is

Table 1
Structural properties of sorbents used

Sorbent	Base matrix	Mean particle diameter (μm)	ϵ_p	
			(0.36 nm)[a]	(1.77 nm)
TosoHaas SP650C	Vinyl polymer	110[b]	0.630	0.535
TosoHaas SP550C	Vinyl polymer	110[b]	0.701	0.470
Pharmacia SP Sepharose FF	Agarose	92[b]	0.844	0.694
EMD Fractogel SO_3^- 650M	Vinyl polymer	70[c]	0.685	0.436
Baker Carboxy-Sulfone	Silica	40[d]	0.684	0.480
Biosepra SP Spherodex M	Silica	90[e]	0.579	0.484

[a] Value represents viscosity radius of SEC probe for which porosity was determined. From ref. [4].
[b] Average of particle size distribution.
[c] Average of particle size distribution of TosoHaas SP650M (same base matrix).
[d] Reported by manufacturer.
[e] Estimated by optical microscopy.

derivatized to provide ''tentacles'' to increase the adsorbent affinity and capacity [24]. Biosepra SP Spherodex is a dextran-coated silica material.

Detailed pore size distribution information has been obtained by inverse size-exclusion chromatography (SEC) [4]. Two porosities are shown for each material in Table 1. The first is that based on the smallest SEC probe (glucose), and thus provides a measure of the total porosity. However, the smallest pores are inaccessible to proteins, and thus a more appropriate measure of the porosity for lysozyme chromatography is one based on an SEC probe closer in size to lysozyme [25]; the values for a dextran standard with a viscosity radius of 1.77 nm are used for this purpose.

All resins were pretreated with the appropriate buffer prior to experimentation. All experimental data were collected on a sorbent settled volume basis.

2.2. Apparatus

Batch adsorption experiments were performed using an experimental setup similar to that used in numerous previous studies. The contacting vessel was a 100 ml glass beaker to which an entrance port was added near the base. The protein concentration in the vessel was monitored by continuously withdrawing a small sample through a solvent filter (Upchurch Scientific, Model A302) with 10 μm pores to keep the particles in the vessel. The protein solution withdrawn was circulated, using a peristaltic pump (Cole Parmer, Model 7520-35), through a spectrophotometer (Isco, Model 226), before it was returned to the beaker. The absorbance was measured at 254 nm in a cell of path length 1 mm; linearity of the absorbance with protein concentration was assured under these conditions. Measurements were recorded through a computer data acquisition program (Isco ChemResearch). The hold-up volume in the PTFE circulation loop was about 1.3 ml, resulting in a circulation time of about 6–8 s at the flow rates used in these experiments (9–13 ml/min).

The suspension was agitated by a PTFE paddle driven from above by an electric mixer via a glass shaft (Kontes, Vineland, NJ, USA). Magnetically driven stirrers were avoided to minimize particle breakage. Mixing was further improved by four removable Delrin baffles around the periphery of the vessel. To minimize protein denaturation at the solution–air interface, especially in the presence of a vortex, a floating Delrin cap was used. Two holes in the cap allowed for the removal of solvent through the filter and introduction of the stirring shaft from above.

2.3. Procedures

In each experiment, the baffle-containing vessel was loaded with a known volume of buffer (approx. 74–79.5 ml). Baseline measurements were made once the stirrer and pump were turned on. To achieve the desired initial protein concentration, approximately 0.5 to 6.0 ml of a concentrated lysozyme solution (~40 mg/ml) was added to the vessel, giving a total volume of 80 ml. One milliliter of the vessel contents was withdrawn and stored in a 1.5 ml polypropylene centrifuge tube for subsequent off-line absorbance measurement to provide an exact value for the initial protein concentration.

To start the uptake portion of the experiment, 1.6 ml of a 1:1 (v/v) suspension of the stationary phase was quickly introduced. Data were recorded for the first hour, and for an additional hour or two if a significant amount of uptake appeared still to be occurring. Changes in bulk solution concentration were typically small, although not insignificant, at longer times. To avoid particle breakage during extended agitation, the experiment was terminated after 3 h at most. The particles and the suspending protein solution were transferred to a 125 ml Nalgene bottle to allow adsorption to proceed to completion. The final concentration was measured 24 h later to obtain an equilibrium value of protein uptake for constructing an adsorption isotherm. Equilibrium adsorbed amounts q^* were calculated by material balance from the initial (c_0) and final (c^*) protein concentrations, the solution volume, V_0, and the adsorbent settled volume, v_{ads}:

$$q^* = \frac{(c_0 - c^*)V_0}{v_{ads}} \quad (1)$$

In some cases additional solution depletion/batch adsorption experiments were performed to provide additional isotherm points. Protein solutions of vari-

ous volumes and concentrations ranging from 0–3 mg/ml were prepared in 15 and 50 ml graduated centrifuge tubes, using 0.3 and 1.0 ml respectively of 1:1 particle suspension. The vials were sealed and mixed by gentle tumbling for 24 h before final concentration measurements were made.

3. Theory

As discussed in the Introduction, a variety of models have been used to characterize transport of proteins and other solutes in porous particles. Since we are interested mainly in the comparative behavior of different stationary phases, it is desirable to fit the experimental data in terms of a minimal number of parameters, the values of which can then be compared for the different materials. We have done so for two of the most frequently cited models, namely the pore diffusion model and the homogeneous diffusion model. In each case we have treated only one parameter, an effective diffusivity, as being adjustable. In some cases we also combined the models to allow effectively for parallel pore and ''surface'' diffusion [21,22], but the additional degree of freedom provided by this two-parameter model only sometimes resulted in better fits, and then at the cost of more questionable physical interpretation. The results of these calculations are thus not presented here. Even for the one-parameter models, however, we are not yet in a position to undertake a reliable effort in model discrimination. Nevertheless, our previously acquired information on sorbent material properties allows us to correlate the effective diffusivities from the one-parameter models to the structural characteristics of each adsorbent.

3.1. Pore diffusion model

In the pore diffusion model, diffusion is assumed to take place in the liquid-filled pores, accompanied by adsorption on the bounding pore walls. This behavior is described by the diffusion equation

$$\epsilon_p \frac{\partial c}{\partial t} = \epsilon_p \frac{D_p}{r^2} \frac{\partial}{\partial r} r^2 \frac{\partial c}{\partial r} - \frac{\partial q}{\partial t} \tag{2}$$

where c and q, the concentration of protein in the pores and adsorbed respectively, are expressed as functions of radial position r and time t. D_p is the effective pore diffusivity, and ϵ_p is the internal porosity of the stationary phase. c is expressed per unit accessible pore volume, while q is expressed per unit settled volume of sorbent, including both solid and pores.

The form in which the diffusivity is expressed in Eq. (2) explicitly shows only the dependence on effective porosity, ϵ_p (including partitioning); the effects of hindrance and tortuosity are lumped into the effective pore diffusivity D_p as $D_p = K_d D_m/\tau$, where K_d reflects the hindrance, τ the tortuosity, and D_m the diffusivity in free solution. The reason for not including K_d and τ explicitly is that they are more difficult to predict for materials with pore structures as complex as those examined here. The dependence on ϵ_p is more straightforward, although the porosity is effectively reduced at high solute loadings as a result of the presence of adsorbed protein. The net contribution of the various effects that retard protein transport can be assessed from the ratio of the value of D_p estimated from our experiments to the free solution diffusivity D_m.

Adsorption is assumed to be at equilibrium locally. Thus, the amount of q at a given radial position r and time t is fixed by the isotherm relation

$$q(r,t) = q^*[c(r,t)] \tag{3}$$

allowing the $\partial q/\partial t$ term to be rewritten in terms of $\partial c/\partial t$ and combined with the derivative on the left-hand side of Eq. (2). The isotherm Eq. (3) is almost always expressed in the form of the Langmuir isotherm, the assumptions underlying which are rarely satisfied for protein adsorption. Furthermore, protein adsorption isotherms often deviate noticeably from the Langmuir form. We thus fitted our experimental isotherm data to a form suggested by a novel isotherm equation that we have developed based on a colloidal theory of protein adsorption [26]:

$$c^* = \frac{q^*}{K_{\text{eq}}} \exp[B\sqrt{q^*}\exp(-\gamma/\sqrt{q^*})] \tag{4}$$

Here K_{eq} is the adsorption equilibrium constant in the dilute (Henry's Law) limit, and B and γ are lumped parameters that characterize protein–protein electrostatic repulsion and the protein packing on the

surface. Despite the physical basis for this isotherm equation, in the present work we treat it simply as a functional form to which our data are fitted.

Eq. (2) must be solved subject to boundary and initial conditions expressing the flux at the surface of particle,

$$\epsilon_p D_p \cdot \frac{\partial c}{\partial r} = k_f(c_b - c) \quad \text{at } r = R \tag{5}$$

the symmetry at the center of the particle,

$$\frac{\partial c}{\partial r} = 0 \quad \text{at } r = 0 \tag{6}$$

and the initial absence of protein from the particle interior,

$$c = q = 0 \quad \text{at } t = 0 \tag{7}$$

In addition, because of the finite volume of the contacting vessel, a mass balance on the protein,

$$3\frac{v_{ads}}{R^3}\int_0^R (\epsilon_p c + q) r^2 \, dr + c_b V_0 = c_0 V_0 \tag{8}$$

is used to calculate the protein concentration in the supernatant. It is at this level that the calculations are compared to experimental measurements. In these equations, k_f is the mass transfer coefficient of protein from the bulk to the surface of the particle, c_b is the supernatant protein concentration and c_0 is its initial value. The particles are assumed to be monodisperse spheres of radius R. We have also performed calculations that incorporate more complete information on the particle size distribution, but the resulting effects on estimated diffusivities are quite small, and were not incorporated in our parameter estimation in the interest of computational economy.

Because of the nonlinearity of the adsorption isotherm, the equations were solved numerically, using a finite difference scheme on a non-uniform grid. D_p was estimated by least-squares minimization of the difference between the experimental and the numerically calculated c_b's at the t values for which experimental measurements were available. Two non-linear least-squares procedures were used, viz. the Nelder–Mead Simplex algorithm [27] for initial estimates, followed by the Levenberg–Marquardt algorithm [28] for final estimates. The mass transfer coefficient k_f was not treated as adjustable, but was calculated for the mean particle size (Table 1) from the correlation [29]

$$k_f = \frac{D_m}{R} + 0.31 \cdot \left(\frac{\mu}{\rho D_m}\right)^{-2/3} \left(\frac{\Delta\rho \ \mu g}{\rho^2}\right)^{1/3} \tag{9}$$

where μ and ρ are the fluid viscosity and density respectively, $\Delta\rho$ is the density difference between the fluid and the particles and g is the gravitational acceleration. This correlation has been used previously in studies of this kind, e.g., [19].

3.2. Homogeneous diffusion model

In the homogeneous diffusion model, all protein within the particle, whether free or adsorbed, is lumped into the single quantity q (still a function of r and t). Protein diffusion within the particle is then assumed to be governed by the gradient in the total protein concentration q, resulting in the governing equation

$$\frac{\partial q}{\partial t} = \frac{D_h}{r^2} \cdot \frac{\partial}{\partial r} \cdot r^2 \frac{\partial q}{\partial r} \tag{10}$$

The effective homogeneous diffusion coefficient D_h will typically be smaller than D_p for a corresponding system, because of the concentrating effect of adsorption: q is generally locally higher than c, and the gradient $\partial q/\partial r$ is correspondingly higher than $\partial c/\partial r$.

Eq. (10) is to be solved subject to boundary, initial and mass balance conditions adapted from those for the pore diffusion model. The modifications are straightforward, the most important being to the surface flux Eq. (5), which now incorporates the isotherm information

$$D_s \frac{\partial q}{\partial r} = k_f[c_b - c^*(q)] \quad \text{at } r = R \tag{11}$$

Here $c^*|_R$ is the concentration of protein in solution that is in equilibrium with the total concentration q at the particle surface.

4. Results and discussion

4.1. Isotherms

Adsorption isotherm data were obtained for lysozyme on all the adsorbents under different salt

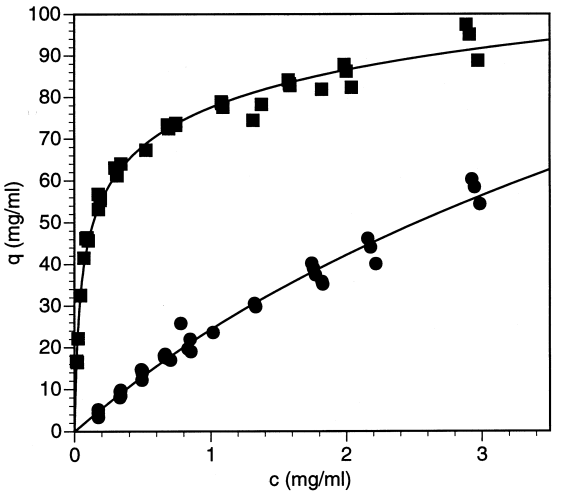

Fig. 1. Adsorption isotherms for lysozyme on Pharmacia SP Sepharose FF at pH 7 and 0.1 *M* (squares) and 0.2 *M* (circles) NaCl. Solid lines are fits based on Eq. (4) with parameters as given in Table 2.

conditions. Typical data are those shown for SP Sepharose in Fig. 1. The usual trend is observed in which an increase in the salt concentration leads to a decrease in the initial slope of the isotherm, which is pronounced enough that a plateau is not always reached within the concentration range studied. Furthermore, even where the isotherm does level off to some extent, a well-defined plateau is not always present.

The qualitative observations of isotherm shape also have implications for the quantitative fitting of an isotherm equation to the data. Although the Langmuir equation is able to fit some data sets adequately, experimental data sets generally diverge from the Langmuir form by showing less deviation from linearity at low coverages and more deviation, i.e., a ''softer'' form, at higher coverages. As shown in Fig. 1, however, the form given in Eq. (4) is able to follow the experimental data quite well. This is due, in part, simply to the flexibility afforded by having three parameters instead of the two in the Langmuir equation, but the main point is that the isotherm data are suitably described in analytical form.

The fitted parameters for all the isotherm data are given in Table 2. The equilibrium constant K_{eq} decreases with increasing salt concentration for each

Table 2
Adsorption isotherm fit parameters

Sorbent	[NaCl] (M)	K_{eq}	B	γ
SP650C	0.1	683	1.85	5.07
SP550C	0.1	16200	4.91	24.3
SP550C	0.2	465	8.48	33.6
SP Sepharose	0.1	1080	4.43	23.8
SP Sepharose	0.2	27.0	0.221	11.4
Carboxy-Sulfone	0	6810	1670	120
Carboxy-Sulfone	0.1	1670	293	83.5
EMD SO_3^-	0.1	2820	98.5	58.2
EMD SO_3^-	0.2	192	104	61.7
SP Spherodex	0	9000	42.3	44.8
SP Spherodex	0.1	6650	2.81	12.2

adsorbent as expected, and the rank order when all the adsorbents are compared at the common salt concentration of 0.1 *M* corresponds closely to that found for k' values in column isocratic elution experiments [5]. Although k' data were not obtained at 0.1 *M* in that work because of the extremely strong retention that would have resulted, the ranking at higher salt concentrations was the same as that for K_{eq} here except for the reversal of the order of the Carboxy-Sulfone and the EMD SO_3^- materials. In addition, for those equations for which K_{eq} and k' data are available, the quantitative agreement is very good.

The values of B and γ, including the trends with salt concentration, are less easily interpreted. There is more scatter in B than in γ, reflecting the different physical significance of the two parameters. In the idealized model [26], B characterizes the mutual exclusion of particles from the surface, which, in the porous adsorbents used here, would also depend on the detailed pore structures; this would explain the wide variation among the different materials. γ, on the other hand, characterizes mainly the protein and the solvent in the idealized model, although it depends also on the total adsorbent capacity; the variation here is much smaller.

The resulting isotherms are shown for the 0.1 *M* NaCl data in Fig. 2; only the fitted curves are shown in the interest of clarity. The plateau levels, which provide a measure of the adsorption capacity, cover about a five-fold range. The capacities are, in general, correlated with the affinities (characterized by the initial slopes of the isotherms); this is to be expected, as both should depend on the phase ratio.

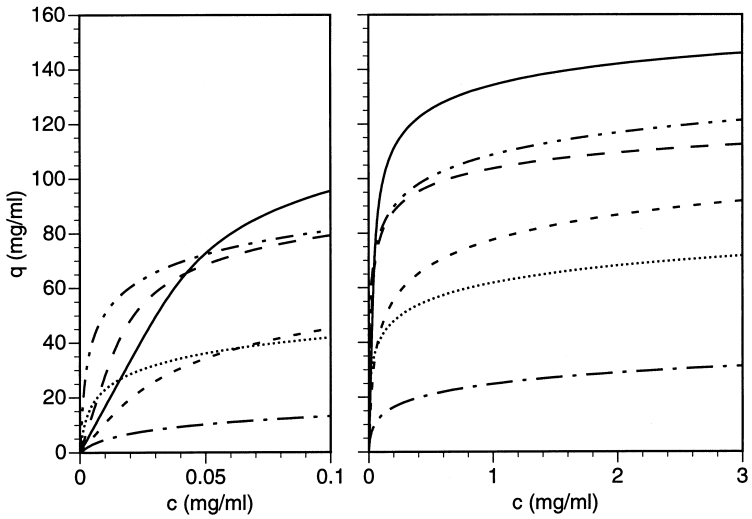

Fig. 2. Comparison of lysozyme adsorption isotherms on different stationary phases at pH 7 and 0.1 *M* NaCl. Lines show fits of Eq. (4) with parameters as given in Table 2. Key: SP650C, — - — SP550C, —- - - —; SP Sepharose. – –: Carboxy-Sulfone, ———; EMD SO_3^-, — — SP Spherodex, ···.

The correlation is not perfect, however, especially among the high-affinity TosoHaas SP550C, Carboxy-Sulfone and Spherodex adsorbents.

Quantitative insight into these isotherm trends can be obtained by correlating them with structures of the stationary phases. The initial slopes of the isotherms are analyzed in this way elsewhere [5], while here we focus on the stationary phase capacity. Table 3 lists, for each of the stationary phases, a comparison of the static capacity with various structural parameters determined separately [4]. The accessible volumes and surface areas are those for a dextran probe of viscosity radius 1.77 nm, consistent with the values shown for the porosities in Table 1. The capacities shown characterize the upper limit of the plateau regions shown in Fig. 2.

Table 3 shows the capacities to correspond to a wide range of effective intrapore concentrations, the highest representing effective volume fractions of about 50%. In contrast, the capacities are quite well correlated with the accessible surface area for adsorption. The surface coverages are all in the vicinity

Table 3
Comparison of static capacities at 0.1 *M* with structural parameters of different stationary phases [4]

Sorbent	Capacity (mg/cm^3)[a]	Mean pore radius (nm)	Specific pore volume (cm^3/cm^3)[b]	Specific surface area (m^2/cm^3)[c]	Pore concentration (mg/cm^3)[d]	Surface concentration (mg/m^2)
SP650C	31	76.6	0.316	19.3	98	1.61
SP550C	121	8.8	0.290	81.6	417	1.48
SP Sepharose	92	24.7	0.451	42.5	204	2.16
Carboxy-Sulfone	146	12.6	0.250	53.6	584	2.72
EMD SO_3^-	112	16.5	0.251	58.9	446	1.90
SP Spherodex	72	34.3	0.305	34.2	236	2.10

[a] Per unit settled volume, characterized by q at 3 mg/ml lysozyme, from isotherm equation.
[b] Accessible pore volume (for 1.77 nm probe) per unit packed volume.
[c] Accessible surface area per unit settled volume.
[d] Per unit accessible pore volume.

of 2 mg/m^2, which agrees well with both coverages measured experimentally by direct methods and coverages calculated for close packing of lysozyme on a planar surface [30–32]. There are uncertainties in these calculations arising especially from the assumption of simple cylindrical pores. This assumption is particularly questionable for gel-based materials such as Sepharose and for the tentacular EMD SO_3^-, and the irregular nature of the internal surface of silica may explain the rather high apparent surface concentration found for the Carboxy-Sulfone. Despite these uncertainties, the results indicate that adsorbent capacities are determined largely by the surface area accessible for adsorption by the protein of interest, and that the high effective concentrations can be explained directly by adsorption rather than partitioning capacity. Thus the appropriate phase ratio to use for analysis of ion-exchange capacity is based on surface area rather than volume. As discussed elsewhere, the affinities appear to be influenced much more strongly by the nature of the adsorbent, which affects the protein–adsorbent interaction [5].

4.2. Uptake data

Least-squares fits were performed on all the data sets with both the pore and homogeneous diffusion models. A representative group of data sets is shown in Fig. 3 for fits of the pore diffusion model to uptake data on TosoHaas SP650C at 0.1 *M* NaCl. The data are presented in terms of the protein concentration in the supernatant, normalized to the initial value to allow all the sets to be presented on the same plot. The fits were performed for different times in order to stress data at shorter times, for two reasons. The first was simply so that the estimate of the diffusivity would be based primarily on the period during which the bulk of the uptake actually occurred. The second was that because of scatter in the isotherm data and the additional small amount of uptake that took place over very long time periods in our isotherm data acquisition, the apparent asymptote within data windows such as that shown in Fig. 3 often differed from that represented by the analytical isotherm equation. Such discrepancies are apparent towards the end of the fit periods shown. Including data at longer times in the fitting procedure would bias the estimate of the diffusivity unreasonably.

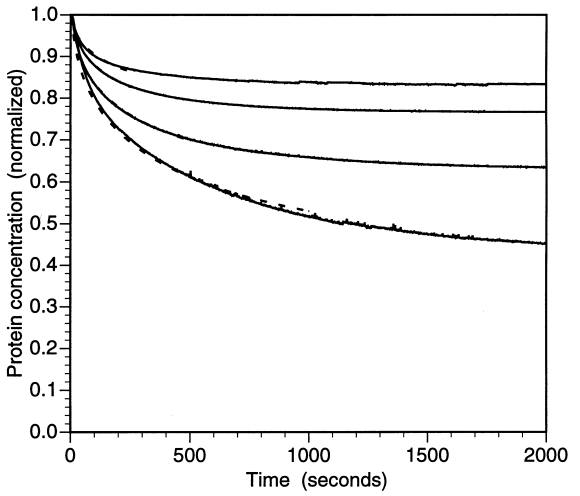

Fig. 3. Fits of pore diffusion model to lysozyme uptake data on TosoHaas SP650C at pH 7 and 0.1 *M* NaCl. Experimental data, solid lines; model fits, broken lines. Initial protein concentrations (from top): 1.36, 0.98, 0.48, 0.24 mg/ml.

Fig. 4 shows the estimates of the diffusivities obtained for data at 0.1 *M* NaCl for the runs for which the fits were judged reasonable; the quality of fit shown in Fig. 3 is typical. The range of dif-

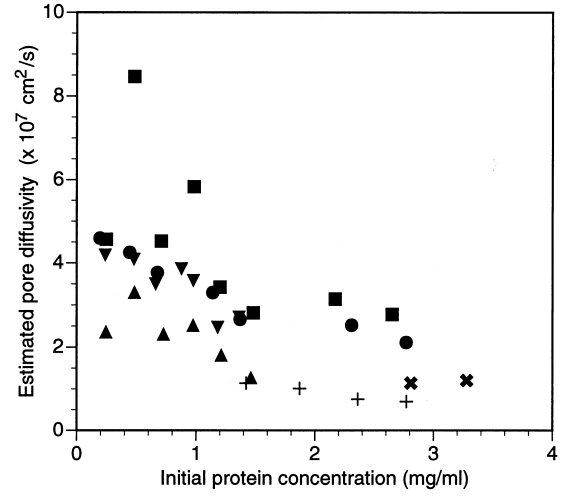

Fig. 4. Estimated pore diffusivities for lysozyme uptake into various stationary phases at pH 7 and 0.1 *M* NaCl. Key: SP650C, ▼; SP550C, ▲; SP Sepharose, ■; Carboxy-Sulfone, +; EMD SO_3^-,●; SP Spherodex, ×.

fusivities obtained can be judged relative to that in free solution, viz. $11.3 \cdot 10^{-7}$ cm^2/s [25]. The fitted values almost all lie between 0.6 and $6 \cdot 10^{-7}$ cm^2/s, corresponding to effective tortuosities between about 2 and 20. There is a clear but weak trend for the diffusivities measured on any one stationary phase to decrease with increasing protein concentration. This may be due to protein–protein interactions, including steric, electrostatic and hydrodynamic effects. Another contribution may come from the pore constriction that results from protein adsorption; although the diffusivities seem to decrease even in the plateau region of the isotherm in some cases, this is due in part to the fact that the abscissa is the initial protein concentration in the supernatant.

In comparing the diffusivities to the stationary phase properties (Table 3), there appear to be different structural factors that can contribute to the transport rate. Mean pore size can clearly play a role, as is seen most clearly by comparing the two TosoHaas materials, with the wide-pore SP650 displaying diffusivities about double those of the narrow-pore SP550. However, other pore structure characteristics may be more important for all but truly restrictive pores. The EMD SO_3^- diffusivities very nicely parallel the SP650 ones despite the appreciable reduction in mean pore size and the increases in affinity and capacity afforded by the ''tentacle'' derivatization. The higher diffusivities seen in SP Sepharose than in SP Spherodex, despite the larger mean pore size of the latter material, suggest that a critical structural feature is pore connectivity. The agarose matrix on which Sepharose is based has a very open gel structure compared to the silica support of Carboxy-Sulfone. The resulting high degree of connectivity allows constrictions to be circumvented, so that pore occlusions are less likely to limit transport. The gel structure of course raises the question of whether Sepharose should really be described in terms of ''pores'' such as those implied in fitting the inverse SEC data [4,33], but the measure obtained of the size distribution should be a reasonable approximation.

Another relevant parameter may be adsorption affinity, with the higher affinities, as characterized by K_{eq} for example, correlated with lower diffusivities. This correlation holds up even if the affinities are corrected for accessible surface area, and it may be a contributing factor in the contrast between the two TosoHaas materials discussed above in the context of mean pore size. Adsorption affinity may be a factor if protein molecules penetrate the particles by virtue of multiple successive cycles of diffusion, adsorption and desorption, since desorption would be slow under high-affinity conditions.

Clear trends are also apparent in the parameter fits obtained using the homogeneous diffusion model (Fig. 5). The diffusivities are now generally about two orders of magnitude lower than the pore diffusivities, and there is a consistent, and in some cases strong, increase in the estimated diffusivity with increasing protein concentration. These features are a result of the nature of the homogeneous diffusion model in basing the protein flux on the overall intraparticle concentration rather than on the concentration of just the unadsorbed protein; the total intraparticle concentrations, and hence concentration gradients, are much higher as a result of adsorption. This effect can be seen in explicit quantitative terms most easily for the limiting case of a linear adsorption isotherm and local adsorption equilibrium: the effective homogeneous and pore diffusion coefficients are related by $D_h = \epsilon_p D_p / (\epsilon_p + K_{eq})$ [34]. This result thus suggests that the low values of D_h are due to the very high values of K_{eq} (Table 2).

Most of our uptake experiments were performed at

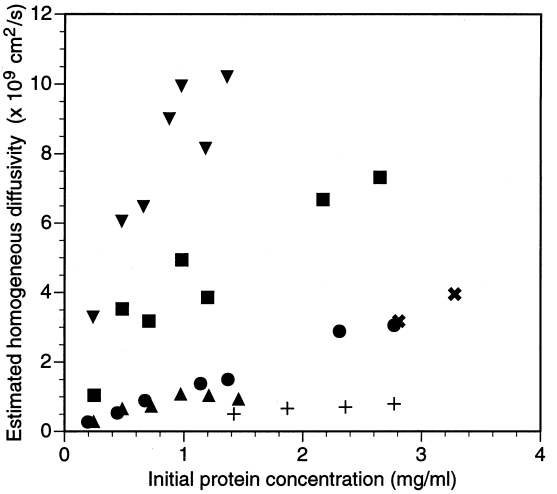

Fig. 5. Estimated homogeneous diffusivities for lysozyme uptake into various stationary phases at pH 7 and 0.1 *M* NaCl. Key as in Fig. 4.

initial protein concentrations well beyond the linear region of the isotherm, so despite the decrease in c over the course of the experiment, the limiting result for linear isotherms will underpredict D_h because of the convex upward form of the isotherm. A generalization of the linear result to arbitrary isotherms is that D_h is given locally by $D_h = \epsilon_p D_p / [\epsilon_p + (dq^*/dc^*)]$, which implies that it varies with both time and position. If this expression is used to estimate D_h at the initial protein concentration, i.e., furthest out on the plateau, the gradient in the denominator will be smaller than any average over the course of the experiment, and thus D_h will be overestimated. Thus to provide an intermediate estimate of whether the trends in Fig. 5 are reasonable, (q/c) at the initial condition of the experiment was used to correct for the enrichment due to adsorption. The resulting quantity $D_h[\epsilon_p + (q/c)_{\text{init}}]/\epsilon_p$ is shown in Fig. 6 for the experiments for which D_h data are presented in Fig. 5. The resulting plot is remarkably similar, both qualitatively and quantitatively, to that of D_p (Fig. 4), the most noticeable difference between the two plots being that the results for TosoHaas SP650C and for EMD SO_3^- are no longer aligned.

These results indicate that, despite the distinct differences between the two models and the large qualitative and quantitative discrepancies between the patterns in the two diffusivity plots, the two models actually provide very similar representations of the data. Thus either model is capable of describing the uptake results for which diffusivity estimates are shown, which include a large majority of the experiments performed. The only stationary phases for which good fits could not be obtained in several cases were the Carboxy-Sulfone and Spherodex materials, both of which, interestingly, are based on silica supports.

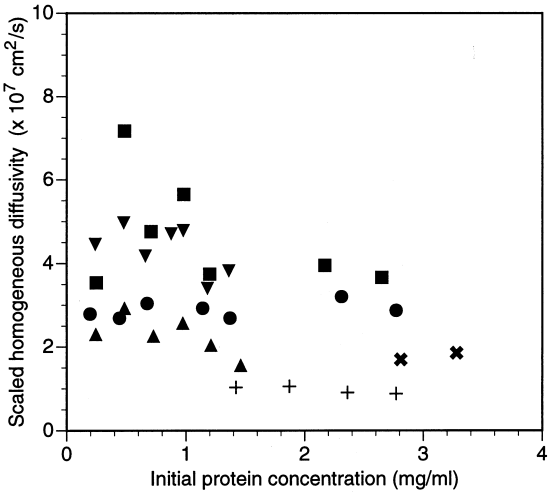

Fig. 6. Estimated homogeneous diffusivities from Fig. 5, rescaled to account for ratio of adsorbed and free protein concentrations. Key as in Fig. 4.

That there is no clear basis for model discrimination between the two models also means that the true physical processes occurring within the particles cannot be inferred directly from the data. As pointed out by Weaver and Carta [17], the two modes of behavior can be distinguished by plotting the experimental data not in terms of the residual supernatant protein concentration, but in terms of the amount of protein taken up, which can be calculated from a mass balance. A ''signature'' of homogeneous diffusion is that the uptake curves overlap for concentrations in the plateau region of the isotherm. This behavior indicates that the uptake rate is independent of the free protein concentration, and instead dependent on the total amount of protein in the particles. We did not see clear evidence of such behavior for any of the stationary phases that we investigated. Weaver and Carta saw such behavior for a Biosepra Hyper D material, which comprises a rather dense gel within silica pores and thus may be expected to display transport behavior that is dominated by adsorbed protein. In general, though, determining the physical mechanisms of transport and adsorption is likely to require independent experiments, e.g., using microscopy methods [35–38]. It appears that modelling of protein uptake can be performed equivalently using either mode, the pore diffusion model having a clearer physical basis.

All the dynamic uptake results presented thus far were for experiments performed at 0.1 *M* NaCl. We also investigated the effect on uptake rates of increasing or decreasing the salt concentration. Fig. 7 shows results for the pore diffusion model for all the adsorbents except TosoHaas SP650C. The clear trend is for the effective diffusivity to increase with increasing salt concentration. It is unlikely that this is due to a direct salt effect on protein diffusion over such a small range of salt concentration [39]. Instead, it is likely that the salt effect is related to the

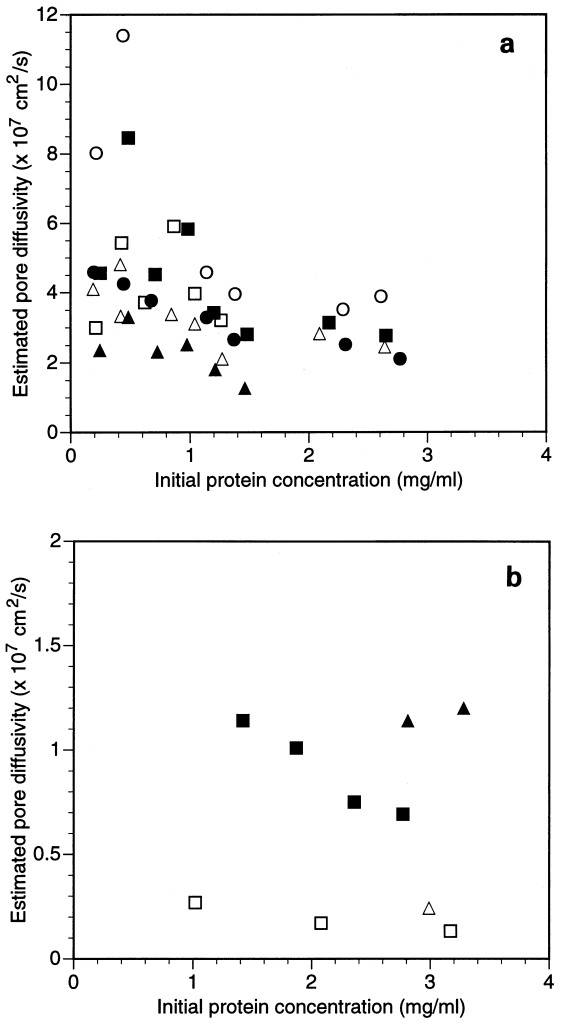

Fig. 7. Salt effect on estimated pore diffusivities for lysozyme uptake into various stationary phases at pH 7 and 0.1 *M* NaCl. (a) 0.1 *M*, closed symbols; 0.2 *M*, open symbols. Key: SP550C, △; SP Sepharose, ■; EMD SO_3^-, ●. (a) 0 *M*, closed symbols; 0.1 *M*, open symbols. Key: Carboxy-Sulfone, ■; SP Spherodex, △.

modulation of protein–protein and protein–surface interactions. There are several mechanisms to be considered:

(1) As the salt concentration is decreased, electrostatic protein–protein repulsion becomes stronger because of the reduced screening, and this may cause the diffusion of an individual protein molecule to be influenced by other nearby molecules. This effect would of course be enhanced as the protein concentration increases. However, strong repulsion between particles in simple gradient diffusion *increases* the effective diffusion coefficient [40].

(2) The repulsion between free, diffusing protein molecules and their adsorbed counterparts is increased at lower salt concentrations. This is conceptually similar to protein partitioning and transport in a pore of like charge, which results in a reduction in diffusivity with increasing repulsion [9].

(3) Protein transport within the particle may occur in part via a mechanism of successive desorption, diffusion and readsorption. In this case the stronger binding at lower salt concentrations would lead to slower desorption, which would retard the overall process.

(4) If true surface diffusion occurs, it too may be retarded by the stronger binding that occurs at lower salt concentrations.

Again it will be difficult to determine which effects are dominant simply from uptake experiments, and indeed resolving some of these issues may be impossible within the limitations of current experimental capabilities.

5. Conclusions

We have presented comparative results of lysozyme adsorption equilibrium and mass transfer on six different cation exchangers. There are clear differences among the results on the different materials, most of which can be correlated with stationary phase structural parameters. The protein adsorption capacity of an adsorbent is strongly correlated with the accessible surface area, and less so with the intrinsic adsorption affinity. Uptake dynamics are influenced to a large extent by mean pore size, but other structural parameters, such as pore connectivity and adsorption affinity, also play a role. The importance of the pore size distribution, and not just the mean pore size, is borne out by the central role played by the accessible pore space, which differs for proteins of different sizes. More detailed information on the pore size distributions of different adsorbents is presented elsewhere [4], and can be used to estimate structural parameters for proteins other than lysozyme.

Various different mass transfer models have been used to describe uptake into chromatographic par-

ticles in the past. Our results show that more than one such model may often be capable of describing uptake data equally well, without resolving questions regarding the physical mechanisms of coupled diffusion and adsorption. Independent methods, capable of higher resolution, are necessary to explore this issue further. For the present, however, our results facilitate approximate prediction of stationary phase properties that can be useful in stationary phase selection and optimization of operating conditions.

Acknowledgements

We are grateful to Mark R. Schure and Saurabh A. Palkar for assistance in implementing the parameter estimation routine. We also thank TosoHaas and EM Industries for gifts of stationary phase materials.

References

[1] K.K. Unger, R. Janzen, J. Chromatogr. 373 (1986) 227.
[2] E. Boschetti, J. Chromatogr. 658 (1994) 207.
[3] V.B. Lawlis, H. Heinsohn, LC·GC 11 (1993) 720.
[4] P.D. DePhillips, A.M. Lenhoff (1998) in preparation.
[5] P.D. DePhillips, A.M. Lenhoff (1998) in preparation.
[6] R.D. Whitley, K.E. Van Cott, J.A. Berninger, N.-H.L. Wang, AIChE J. 37 (1991) 555.
[7] G. Guiochon, S.G. Shirazi, A.M. Katti, Fundamentals of Preparative and Non-Linear Chromatography, Academic Press, San Diego, CA, 1994.
[8] J.C. Bellot, J.S. Condoret, Process Biochem. 26 (1991) 363.
[9] W.M. Deen, AIChE J. 33 (1987) 1409.
[10] E.M. Renkin, J. Gen. Physiol. 38 (1954) 225.
[11] J.H. Knox, H.P. Scott, J. Chromatogr. 316 (1984) 311.
[12] C.N. Satterfield, Mass Transfer in Heterogeneous Catalysis, MIT Press, Cambridge, MA, 1970.
[13] J.H. Petropoulos, A.I. Liapis, N.P. Kolliopoulos, J.K. Petrou, N.K. Kanellopoulos, Bioseparation 1 (1990) 69.
[14] A. Johnston, M.T.W. Hearn, J. Chromatogr. 557 (1991) 335.
[15] B.H. Arve, A.I. Liapis, AIChE J. 33 (1987) 179.
[16] G.L. Skidmore, B.J. Horstmann, H.A. Chase, J. Chromatogr. 498 (1990) 113.
[17] L.E. Weaver, G. Carta, Biotechnol. Prog. 12 (1996) 342.
[18] M.A. Fernandez, G. Carta, J. Chromatogr. A 746 (1996) 169.
[19] B.J. Horstmann, H.A. Chase, Chem. Eng. Res. Des. 67 (1989) 243.
[20] A. Tongta, A.I. Liapis, D.J. Siher, J. Chromatogr. A 686 (1994) 21.
[21] G.F. Bloomingburg, G. Carta, Chem. Eng. J. 55 (1994) B19.
[22] H. Yoshida, M. Yoshikawa, T. Kataoka, AIChE J. 40 (1994) 2034.
[23] R.K. Lewus, F.H. Altan, G. Carta, Ind. Eng. Chem. Res. 37 (1998) 1079.
[24] W. Muller, J. Chromatogr. A 510 (1990) 133.
[25] T.E. Creighton, Proteins: Structures and Molecular Properties, 2nd ed., W.H. Freeman, New York, 1993.
[26] M.R. Oberholzer, A.M. Lenhoff (1998) submitted for publication.
[27] R. O'Neill, in: P. Griffiths, I.D. Hill (Eds.), Applied Statistics Algorithms, Ellis Horwood, Chichester, 1985, pp. 79–87.
[28] P.R. Bevington, Data Reduction and Error Analysis for the Physical Sciences, McGraw-Hill, New York, 1969.
[29] C.J. Geankoplis, Transport Processes and Unit Operations, 2nd ed., Allyn and Bacon, Boston, MA, 1983.
[30] R.Z. Guzman, R.G. Carbonell, P.K. Kilpatrick, J. Coll. Interf. Sci. 114 (1986) 536.
[31] C.T. Shibata, A.M. Lenhoff, J. Coll. Interf. Sci. 148 (1992) 469.
[32] T. Arai, W. Norde, Coll. Surf. 51 (1990) 1.
[33] L. Hagel, M. Östberg, T. Anderson, J. Chromatogr. A 743 (1996) 33.
[34] O.D. Velev, A.M. Lenhoff, E.W. Kaler (1998) in preparation.
[35] E. Firouztalé, A.P. Scott, S.K. Dalvie, G.M. Von Blohm, AIChE Symp. Ser. 290 (1993) 25.
[36] J.L. Coffman, E.N. Lightfoot, T.W. Root, J. Phys. Chem. B 101 (1997) 2218.
[37] S.A. Palkar, A.M. Lenhoff, Coll. Surf. A 110 (1996) 119.
[38] A. Ljunglöf, R. Hjorth, J. Chromatogr. A 743 (1996) 75.
[39] J.L. Anderson, F. Rauh, A. Morales, J. Phys. Chem. 82 (1978) 608.
[40] W.B. Russel, D.A. Saville, W.R. Schowalter, Colloidal Dispersions, Cambridge University Press, Cambridge, 1989.